Inorg. Chem. **2002**, *41*, 5107–5118

Single-Molecule Magnets: Novel Mn_8 and Mn_9 Carboxylate Clusters Containing an Unusual Pentadentate Ligand Derived from Pyridine-2,6-dimethanol

Colette Boskovic,[1a] Wolfgang Wernsdorfer,[1b] Kirsten Folting,[1a] John C. Huffman,[1a] David N. Hendrickson,*[,1c] and George Christou*[,†,1a]

Department of Chemistry and the Molecular Structure Center, Indiana University, Bloomington, Indiana 47405-7102, Laboratoire Louis Néel-CNRS, BP166, 25 Avenue des Martyrs, 38042 Grenoble, Cedex 9, France, and Department of Chemistry-0358, University of California at San Diego, La Jolla, California 92093-0358

Received March 20, 2002

The reactions of the Mn^{III}_3 and $Mn^{II}Mn^{III}_2$ complexes $[Mn_3O(O_2CEt)_6(py)_3][ClO_4]$ and $[Mn_3O(O_2CEt)_6(py)_3]$ with pyridine-2,6-dimethanol ($pdmH_2$) afford the mixed-valence $Mn^{II}_6Mn^{III}_2$ octanuclear complex $[Mn_8O_2(py)_4(O_2CEt)_8(L)_2][ClO_4]_2$ (**1**) and the $Mn^{II}_7Mn^{III}_2$ enneanuclear complex $[Mn_9(O_2CEt)_{12}(pdm)(pdmH)_2(L)_2]$ (**2**), respectively. Both compounds contain a novel pentadentate ligand, the dianion of (6-hydroxymethylpyridin-2-yl)-(6-hydroxymethylpyridin-2-ylmethoxy)-methanol (LH_2), which is the hemiacetal formed in situ from the Mn-assisted oxidation of $pdmH_2$. Complex **1** crystallizes in the monoclinic space group $P2_1/n$ with the following cell parameters at –160 °C: $a = 16.6942(5)$ Å, $b = 13.8473(4)$ Å, $c = 20.0766(6)$ Å, $\beta = 99.880(1)°$, $V = 4572.27$ Å^3, and $Z = 2$, R (R_w) = 4.78 (5.25). Complex **2**·0.2MeCN crystallizes in the triclinic space group $P\bar{1}$ with the following cell parameters at –157 °C: $a = 12.1312(4)$ Å, $b = 18.8481(6)$ Å, $c = 23.2600(7)$ Å, $\alpha = 78.6887(8)°$, $\beta = 77.9596(8)°$, $\gamma = 82.3176(8)°$, $V = 5076.45$ Å^3, and $Z = 2$, R (R_w) = 4.12 (4.03). Both complexes are new structural types comprising distorted-cubane units linked together, albeit in two very different ways. In addition, complex **2** features three distinct binding modes for the chelating ligands derived from deprotonated $pdmH_2$. Complexes **1** and **2** were characterized by variable-temperature ac and dc magnetic susceptibility measurements and found to possess spin ground states of 0 and 11/2, respectively. Least-squares fitting of the reduced magnetization data gave $S = 11/2$, $g = 2.0$, and $D = –0.11$ cm^{-1} for complex **2**, where D is the axial zero-field splitting parameter. Direct current magnetization versus field studies on **2** at <1 K show hysteresis behavior at <0.3 K, establishing **2** as a new single-molecule magnet. Magnetization decay measurements gave an effective barrier to magnetization relaxation of $U_{eff} = 3.1$ cm$^{-1} = 4.5$ K.

Introduction

The search for new polynuclear Mn carboxylate clusters is presently largely driven by the pursuit of new single-molecule magnets (SMMs).[2−4] These are species that display slow relaxation of magnetization and thus can function as magnetizable magnets below their blocking temperature. This behavior results from a large ground state spin (S) value combined with a large and negative (easy-axis-type) magnetoanisotropy, as measured by the axial zero-field splitting parameter D. This combination leads to a significant barrier to magnetization reversal, its maximum value given by $S^2|D|$ or $(S^2 - {}^1/_4)|D|$ for integer and half-integer spins, respectively. Thus, at low enough temperatures, there is insufficient thermal energy to overcome this anisotropy barrier and the magnetization therefore stays frozen. Experimentally, a single-molecule magnet shows superparamagnet-like properties, exhibiting both a frequency-dependent out-of-phase ac

† Present address: Department of Chemistry, University of Florida, Gainesville, FL 32611-7200.

(1) (a) Indiana University. (b) Laboratoire Louis Néel-CNRS. (c) University of California at San Diego.
(2) Christou, G.; Gatteschi, D.; Hendrickson, D. N.; Sessoli, R. *MRS Bull.* **2000**, *25*, 56.
(3) (a) Sessoli, R.; Tsai, H.-L.; Schake, A. R.; Wang, S.; Vincent, J. B.; Folting, K.; Gatteschi, D.; Christou G.; Hendrickson, D. N. *J. Am. Chem. Soc.* **1993**, *115*, 1804. (b) Sessoli, R.; Gatteschi, D.; Caneschi A.; Novak, M. A. *Nature* **1993**, *365*, 141.
(4) Aubin, S. M. J.; Wemple, M. W.; Adams, D. M.; Tsai, H.-L.; Christou, G.; Hendrickson, D. N. *J. Am. Chem. Soc.* **1996**, *118*, 7746.

10.1021/ic020217p CCC: $22.00
Published on Web 09/13/2002

magnetic susceptibility signal and hysteresis in a plot of magnetization versus magnetic field. In addition, SMMs have been found to display steps in the magnetization hysteresis loops that are due to quantum tunneling of the magnetization.[5] Manganese carboxylate clusters have proved to be the best source of SMMs, with the following four distinct families of such compounds having been identified: $[Mn_{12}O_{12}(O_2CR)_{16}(H_2O)_x]^{n-}$ ($n = 0, 1, 2$; $x = 3, 4$) and their derivatives;[2,3,6−8] distorted-cubane complexes with the $[Mn^{IV}Mn^{III}_3O_3X]^{6+}$ ($X = Cl^-$, Br^-, F^-, O_2CMe^-, etc.) core;[4,9] $[Mn_4(O_2CMe)_2(pdmH)_6]^{2+}$ and the structurally related species $[Mn_4Br_2(H_2O)_2(hmp)_6]^{2+}$ ($pdmH_2$ = pyridine-2,6-dimethanol and hmpH = 2-(hydroxymethyl)pyridine);[10,11] and $[Mn_{12}O_8Cl_4(O_2CPh)_8(hmp)_6]$.[12] Of these four types of complexes, the tetranuclear complexes with the $[Mn^{IV}Mn^{III}_3O_3X]^{6+}$ core and $[Mn_{12}O_{12}(O_2CR)_{16}(H_2O)_x]^-$ possess noninteger spin ground states of $S = 9/2$ and 19/2, respectively, while the others all possess integer spin ground states. SMMs with noninteger spin ground states are of particular interest because they should not display quantum tunneling in zero applied magnetic fields and therefore are potentially useful as memory storage devices.[13,14]

One synthetic methodology that has proved to be extremely useful for the synthesis of new polynuclear complexes is the reaction of a chelating ligand with a preformed Mn-carboxylate cluster that does not already incorporate any chelate ligands. Some of the most successful starting materials employed for this purpose are the trinuclear μ_3-oxido complexes $[Mn_3O(O_2CR)_6(py)_3]^{n+}$ ($n = 0,1$), which have afforded a variety of new complexes ranging in nuclearity from 2 to 10.[15,16] One of the ligands that has previously proved to be useful in these syntheses, giving a number of new compounds, is the anion of 2-(hydroxymethyl)pyridine (hmpH). Recently we have extended our efforts to the related ligand derived from pyridine-2,6-dimethanol ($pdmH_2$), which is of particular interest due to the number of possible binding modes that it may display. Our first efforts[10] with this ligand led to the tetranuclear complex $[Mn_4(O_2CMe)_2(pdmH)_6][ClO_4]_2$, which is a SMM with $S = 8$ or 9.[10] This species was the first crystallographically characterized polynuclear cluster containing a ligand derived from $pdmH_2$. Previously only mononuclear complexes with ligands derived from $pdmH_2$ had been reported. However, it is interesting to note that in these complexes a variety of binding modes are observed for the $pdmH_2$, $pdmH^-$, or pdm^{2-} ligands, which function as tridentate or bidentate chelating ligands or as monodentate ligands binding only through the nitrogen atom.[17−20]

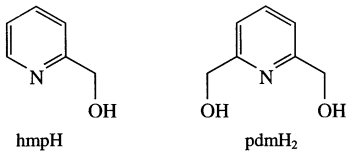

Herein we report the synthesis, structure, and characterization of two new polynuclear Mn-carboxylate clusters synthesized from the reactions of trinuclear Mn complexes with $pdmH_2$. Both of these complexes feature a novel pentadentate ligand formed in situ from $pdmH_2$. In addition, one of these complexes is a high-spin complex with a noninteger spin ground state of $S = 11/2$, and it has been found to be a new example of a half-integer spin single-molecule magnet.

Experimental Section

Syntheses. All manipulations were performed under aerobic conditions, using materials as received. $Mn(O_2CEt)_2 \cdot 4H_2O$ and $[Mn_3O(O_2CEt)_6(py)_3][ClO_4]$ were prepared as described.[21,22] *WARNING: Appropriate care should be taken in the use of $NBu^n_4MnO_4$, and readers are referred to the detailed warning given elsewhere*.[23]

$[Mn_3O(O_2CEt)_6(py)_3]$. To a stirred solution of $Mn(O_2CEt)_4 \cdot 4H_2O$ (4.45 g, 16.3 mmol) in pyridine (40 cm^3) and $EtCO_2H$ (20 cm^3) was added solid $NBu^n_4MnO_4$ (1.38 g, 4.2 mmol) in portions and the solution left to stir overnight. The solution volume was reduced by half, hexanes (90 cm^3) were added, and the resulting solution was placed in the freezer overnight. This led to the formation of a brown crystalline precipitate that was filtered, washed with hexanes, and dried under vacuum; yield 60%. Anal. Calcd (found) for $C_{33}H_{45}N_3O_{13}Mn_3$: C, 46.27 (46.02); H, 5.30 (5.41); N 4.91 (4.90). Selected IR data: 1608 (vs), 1487 (m), 1464 (s), 1448

(5) Friedman, J. R.; Sarachik, M. P. *Phys. Rev. Lett.* **1996**, *76*, 3830. (b) Thomas, L.; Lionti, F.; Ballou, R.; Gatteschi, D.; Sessoli, R.; Barbara, B. *Nature* **1996**, *383*, 145. (c) Tejada, J.; Ziolo, R. F.; Zhang, X. X. *Chem. Mater.* **1996**, *8*, 1784.
(6) (a) Eppley, H. J.; Tsai, H.-L.; de Vries N.; Folting K.; Christou, G.; Hendrickson, D. N. *J. Am. Chem. Soc.* **1995**, *117*, 301. (b) Aubin, S. M. J.; Spagna, S.; Eppley, H. J. Sager, R. E.; Christou, G.; Hendrickson, D. N. *Chem. Commun.* **1998**, 803. (c) Aubin, S. M. J.; Sun, Z.; Pardi, L.; Krzystek, J.; Folting, K.; Brunel, L.-C.; Rheingold, A. L.; Christou, G.; Hendrickson, D. N. *Inorg. Chem.* **1999**, *38*, 5329.
(7) Soler, M.; Chandra, S. K.; Ruiz, D.; Davidson, E. R.; Hendrickson, D. N.; Christou, G. *Chem. Commun.* **2000**, 2417.
(8) (a) Boskovic, C.; Pink, M.; Huffman, J. C.; Hendrickson, D. N.; Christou, G. *J. Am. Chem. Soc.* **2001**, *123*, 9914. (b) Artus, P.; Boskovic, C.; Yoo, J.; Streib, W. E.; Brunel, L.-C.; Hendrickson, D. N.; Christou, G. *Inorg. Chem.* **2001**, *40*, 4199.
(9) Aubin, S. M. J.; Dilley, N. R.; Pardi, L.; Krzystek, J.; Wemple, M. W.; Brunel, L.-C.; Maple, M. B.; Christou, G.; Hendrickson, D. N. *J. Am. Chem. Soc.* **1998**, *120*, 4991.
(10) (a) Brechin, E. K.; Yoo, J.; Huffman, J. C.; Hendrickson D. N.; Christou, G. *Chem Commun.* **1999**, 783. (b) Yoo, J.; Brechin, E. K.; Yamaguchi, A.; Nakano, M.; Huffman, J. C.; Maniero, A. L.; Brunel, L.-C.; Awaga, K.; Ishimoto, H.; Christou G.; Hendrickson, D. N. *Inorg. Chem.* **2000**, *39*, 3615.
(11) Yoo, J.; Yamaguchi, A.; Nakano, M.; Krzystek, J.; Streib, W. E.; Brunel, L.-C.; Ishimoto, H.; Christou G.; Hendrickson, D. N. *Inorg. Chem.* **2001**, *40*, 4604.
(12) (a) Boskovic, C.; Brechin, E. K.; Streib, W. E.; Folting, K.; Hendrickson, D. N.; Christou, G. *Chem. Commun.* **2001**, 467. (b) Boskovic, C.; Brechin, E. K.; Streib, W. E.; Folting, K.; Bollinger J. C.; Hendrickson, D. N.; Christou, G. *J. Am. Chem. Soc.* **2002**, in press.
(13) Di Vincenzo, D. P. *Physica B* **1994**, *197*, 109.
(14) Loss, D.; Di Vincenzo, D. P.; Grinstein, G.; Awschalom, D. D.; Smyth, J. F. *Physica B* **1993**, *189*, 189.
(15) Aromí, G.; Aubin, S. M. J.; Bolcar, M. A.; Christou, G.; Eppley, H. J.; Folting, K.; Hendrickson, D. N.; Huffman, J. C.; Squire, R. C.; Tsai, H.-L.; Wang, S.; Wemple, M. W. *Polyhedron* **1998**, *17*, 3005.
(16) Christou, G. *Acc. Chem. Res.* **1989**, *22*, 328.
(17) Berg, J. M.; Holm, R. H. *Inorg. Chem.* **1983**, *22*, 1768.
(18) Gerber, T. I. A.; Bruwer, J.; Bandoli, G.; Perils, J.; du Preez, J. G. H. *J. Chem. Soc., Dalton. Trans.* **1995**, 2189.
(19) Rochon, F. D.; Beauchamp, A. L.; Bensimon, C. *Can. J. Chem.* **1996**, *74*, 2121.
(20) Rochon, F. D.; Melanson, R.; Kong, P.-C. *Inorg. Chim. Acta* **1997**, *254*, 303.
(21) Aromí, G.; Bhaduri, S.; Artús, P.; Huffman, J. C.; Hendrickson, D. N.; Christou, G. *Polyhedron* **2002**, *21*, 1779.
(22) Vincent, J. B.; Christmas, C.; Chang, H. R.; Li, Q.; Boyd, P. D. W.; Huffman, J. C.; Hendrickson, D. N.; Christou, G. *J. Am. Chem. Soc.* **1989**, *111*, 2086.
(23) Vincent, J. B.; Chang, H. R.; Folting, K.; Huffman, J. C.; Christou, G.; Hendrickson, D. N. *J. Am. Chem. Soc.* **1987**, *109*, 5703.

(s), 1409 (vs), 1366 (s), 1292 (s), 1219 (s), 1155 (m), 1074 (s), 1045 (m), 1035 (m), 942 (w), 1009 (m), 1017 (m), 881 (m), 815 (m), 754 (m), 687 (s), 659 (m), 641 (m), 623 (s), 602 (m), 574 (m), 444 (m) 416 (w).

$[Mn_8O_2(py)_4(O_2CEt)_8(L)_2][ClO_4]_2$ (1). To a solution of $[Mn_3O(O_2CEt)_6(py)_3][ClO_4]$ (0.50 g, 0.52 mmol) in MeCN (20 cm^3) was added $pdmH_2$ (0.11 g, 0.79 mmol), and the resulting solution was stirred overnight and filtered through Celite. Then the filtrate was evaporated to dryness under vacuum. The residue was redissolved in CH_2Cl_2 (5 cm^3) and layered with Et_2O (10 cm^3). After 1 week the resulting solution was removed by pipet from the amorphous solid that had formed and placed in a capped tube. After 3 weeks, crystals were isolated by filtration, washed with Et_2O, and dried under vacuum; yield 10%. A sample for crystallography was obtained by layering the MeCN solution with Et_2O, and the resulting crystals were maintained in contact with the mother liquor to prevent the loss of interstitial solvent. The dried material is hygroscopic, analyzing for **1**·$5H_2O$. Anal. Calcd (found) for $C_{72}H_{98}N_8O_{39}Mn_8Cl_2$: C, 39.13 (39.20); H 4.47 (4.23); N 5.07 (5.04). Selected IR data: 1603 (s), 1581 (s), 1486 (w), 1464 (m), 1445 (m), 1422 (s), 1385 (m), 1372 (m), 1296 (m), 1251 (w), 1221 (w), 1161 (w), 1120 (s), 1108 (s), 1066 (s), 1040 (m), 1018 (m), 883 (w), 800 (w), 755 (w), 735 (w), 706 (m), 623 (m), 593 (m), 495 (w), 439 (w).

$[Mn_9(O_2CEt)_{12}(pdm)(pdmH)_2(L)_2]$ (2). To a solution of $[Mn_3O(O_2CEt)_6(py)_3]$ (0.55 g, 0.64 mmol) in MeCN (20 cm^3) was added $pdmH_2$ (0.25 g, 1.0 mmol), and the resulting solution was stirred overnight, filtered through Celite, and evaporated to dryness under vacuum. The residue was redissolved in MeCN (5 cm^3) and layered with Et_2O (15 cm^3). After several weeks crystals were isolated by filtration, washed with Et_2O, and dried under vacuum; yield 15%. A sample for crystallography was maintained in contact with the mother liquor to prevent the loss of interstitial solvent. Anal. Calcd (found) for $C_{85}H_{111}N_7O_{38}Mn_9$: C, 43.76 (43.63); H 4.80 (4.80); N 4.20 (4.10). Selected IR data: 1760 (m), 1590 (s), 1572 (s), 1551 (s), 1465 (s), 1443 (s), 1413 (s), 1368 (s), 1321 (m), 1287 (s), 1246 (m), 1206 (w), 1162 (m), 1142 (m), 1118 (m), 1098 (m), 1057 (s), 1033 (s), 1016 (m), 939 (m), 881 (m), 811 (m), 789 (m), 762 (m), 695 (m), 679 (m), 639 (m), 612 (m), 585 (w), 570 (m), 536 (m), 514 (m), 494 (m), 462 (m), 440 (m), 414 (w).

X-ray Crystallography. Data were collected on a Bruker platform goniometer equipped with a SMART 6000 CCD detector. Details of the diffractometry, low-temperature facilities, and computational procedures employed by the Molecular Structure Center are available elsewhere.[24] Data collection and structure solution details are listed in Table 1.

For complex **1**, the data were corrected for Lorentz and polarization effects, and equivalent reflections were averaged using the Bruker SAINT software as well as utility programs from the XTEL library. An absorption correction was performed using the SADABS program supplied by Bruker AXS. The structure was solved using SHELXTL and Fourier techniques. Analysis of the data set indicated that the space group was $P2_1/n$. All H atoms were clearly visible and were included as isotropic contributors in the final cycles of refinement. The asymmetric unit consists of the octanuclear cation lying on a center of inversion and one badly disordered $[ClO_4]^-$ anion. In addition, there is one badly disordered solvent molecule in the cell. The pentadentate ligand has disorder in the free hydroxy group; the sum of the occupancy factors for the four alternative oxygen positions is 0.98. A final difference Fourier map was essentially featureless with the largest peak, 1.04 e $Å^{-3}$, lying in the vicinity of the disordered $[ClO_4]^-$ anion.

Table 1. Crystallographic Data for Complexes **1** and **2**·0.2MeCN

	1	**2**
formula[a]	$C_{72}H_{88}Cl_2Mn_8N_8O_{34}$	$C_{89.3}H_{111.6}Mn_9N_{7.2}O_{38}$
fw, g mol^{-1}	2119.93	2388.34
space group	$P2_1/n$	$P\bar{1}$
a, Å	16.6942(5)	12.1312(4)
b, Å	13.8473(4)	18.8481(6)
c, Å	20.0766(6)	23.2600(7)
α, deg		78.6887(8)
β, deg	99.880(1)	77.9596(8)
γ, deg		82.3176(8)
V, $Å^3$	4572.27	5076.45
Z	2	2
T, °C	−160	−157
radiation, Å[b]	0.71073	0.71073
ρ_{calc}, g cm^{-3}	1.613	1.563
μ, cm^{-1}	12.15	11.68
R (R_w), %[c,d,e]	4.78 (6.31)	4.12 (4.03)

[a] Including solvate molecules. [b] Graphite monochromator. [c] $R = 100\sum||F_o| - |F_c||/\sum|F_o|$. [d] $R_w = 100[\sum w(|F_o| - |F_c|)^2/\sum w|F_o|^2]^{1/2}$ where $w = 1/\sigma^2(|F_o|)$.

For complex **2**, an initial survey of a portion of reciprocal space located a set of reflections with a triclinic lattice. Analysis of the full data set using XPREP indicated that the space group was $P\bar{1}$. Data were additionally corrected for absorption effects using the empirical absorption program SADABS. The final averaging of redundant data was carried out using software in the IUMSC XTEL software. The structure was solved by a combination of direct methods (XS in the Bruker software) and difference Fourier techniques. The terminal atoms in three of the $EtCO_2^-$ ligands [C(44), C(54), and C(59)] were disordered. Their occupancies refined to 70, 50, and 65%, respectively. A more complex disorder was observed for the free hydroxy O atom in each of the pentadentate ligands. In each case four possible positions for the atom were located, and the occupancies of the four atoms refined to a sum of 1.03 and 1.09 for O(119) and O(142), respectively. It should be noted that distances and angles involving the disordered atoms should be treated with caution. The asymmetric unit was also found to contain some disordered, mainly unidentified and partially occupied solvent from the crystallization. For the final cycles of least-squares refinement, the H atoms on the enneanuclear complex were introduced in fixed idealized positions with isotropic thermal parameters equal to 1.0 plus the isotropic equivalent of the parent atom. The atoms in the Mn cluster, except for the disordered O atoms, were refined using anisotropic thermal parameters, while the remainder of the atoms were refined with isotropic thermal parameters. The final difference map was essentially featureless, the largest peak was 0.74 e $Å^{-3}$, 0.76 Å from O(120), and the deepest hole was −0.61 e $Å^{-3}$.

Other Measurements. Infrared spectra (KBr disk) were recorded on a Nicolet 510P spectrometer. Elemental analyses were performed by Atlantic Microlab, Inc., Norcross, GA. Variable-temperature dc magnetic susceptibility data down to 1.8 K were collected on powdered microcrystalline samples (restrained in eicosane to prevent torquing) with a Quantum Design MPMS-XL SQUID magnetometer equipped with a 70 kG (7 T) dc magnet. Pascal's constants were used to estimate the diamagnetic correction for each complex, which was subtracted from the experimental susceptibility to give the molar paramagnetic susceptibility (χ_M). Alternating current magnetic susceptibility data were collected on the same instrument employing a 3.5 G field, oscillating at frequencies up to 1500 Hz. Direct current measurements below 1 K were performed

(24) (a) Chisholm, M. H.; Folting, K.; Huffman, J. C.; Kirkpatrick, C. C. *Inorg. Chem.* **1984**, *23*, 1021. (b) Seddon, E. J.; Huffman, J. C.; Christou, G. *J. Chem. Soc., Dalton Trans.* **2000**, 4446.

on single crystals using an array of micro-SQUIDs.[25] The high sensitivity of this magnetometer allows study of single crystals of size 0.01−0.5 mm, for temperatures in the 0.035−6.0 K range, fields up to 1.4 T, and sweep rates up to 10 T/s.[25] The field can be applied in any direction by separately driving three orthogonal coils.

Results

Syntheses. We have previously reported that the reaction of $[Mn_3O(O_2CMe)_6(py)_3][ClO_4]$ with $pdmH_2$ in a 1:3 molar ratio gives the mixed-valence $Mn^{II}_2Mn^{III}_2$ tetranuclear complex $[Mn_4(O_2CMe)_2(pdmH)_6][ClO_4]_2$ (**3**).[10] It is also possible to make the $EtCO_2^-$ and $PhCO_2^-$ analogues of **3** from the corresponding trinuclear complexes.[26] Reducing the proportion of $pdmH_2$ in this reaction from 3 to 1.5 molar equiv per trinuclear complex instead affords a new octanuclear complex. Treatment of a solution of $[Mn_3O(O_2CEt)_6(py)_3][ClO_4]$ in MeCN with 1.5 equiv of $pdmH_2$ followed by filtration, evaporation of the filtrate, redissolution of the residue in CH_2Cl_2, and layering the resulting solution with Et_2O leads to an amorphous solid and a brown homogeneous solution after ~1 week. Subsequent removal of the solution to a capped vessel affords pure crystalline $[Mn_8O_2(py)_4(O_2CEt)_8(L)_2][ClO_4]_2$ (**1**) in 10% yield after several weeks. Decreasing the amount of $pdmH_2$ in the reaction to 1 equiv per trinuclear unit reduces the yield, while using greater than 2 equiv of $pdmH_2$ leads to the isolation of the $EtCO_2^-$ analogue of **3** instead. It was not possible to isolate the $MeCO_2^-$ analogue of complex **1** in pure form from the analogous reaction with $[Mn_3O(O_2CMe)_6(py)_3][ClO_4]$, presumably due to its lower solubility.

Like the related reagent hmpH, the reaction of Mn complexes with $pdmH_2$ affords species with the Mn centers in a lower average oxidation state than in the starting complex. The formation of **1** is summarized in eq 1 and clearly involves reduction of the Mn centers by $pdmH_2$, from an average oxidation state of +3 in the Mn^{III}_3 starting complex to +2.25 in the $Mn^{II}_6Mn^{III}_2$ product. The redox chemistry is also accompanied by fragmentation and structural rearrangement of the Mn-cluster to yield complex **1**.

$$8\,[Mn_3O(O_2CEt)_6(py)_3]^+ + 12\,pdmH_2 \rightarrow 3\,[Mn_8O_2(py)_4(O_2CEt)_8(L)_2]^{2+} + 12\,py + 2\,H_2O + 2\,H^+ \quad (1)$$

The most remarkable feature of this reaction is the in situ formation of the pentadentate ligand L^{2-}, the dianion of (6-hydroxymethylpyridin-2-yl)-(6-hydroxymethylpyridin-2-yl-methoxy)methanol from the reaction of two $pdmH_2$ molecules. The reduction of the Mn^{III} centers to Mn^{II} is associated with oxidation of some of the $pdmH_2$, presumably to the corresponding aldehyde, 6-(hydroxymethyl)-2-pyridinecarboxaldehyde. This subsequently undergoes nucleophilic attack from the alcohol moiety of some of the remaining $pdmH_2$ to yield the hydroxy ether or hemiacetal, L^{2-}. Typically the addition of an alcohol to an aldehyde or ketone to form a hemiacetal and ultimately an acetal occurs slowly in neutral conditions, but more rapidly in the presence of acid, where protonation of the carbonyl group activates it to nucleophilic attack. In the present case the medium is acidic and the Mn complex may also help to catalyze the reaction in addition to oxidizing the $pdmH_2$.

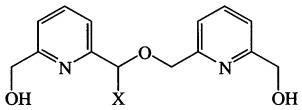

LH_2, X = OH; $L'H_2$, X = H

Complex **2** is prepared from a related reaction employing the mixed-valence trinuclear complex $[Mn_3O(O_2CEt)_6(py)_3]$. Reaction of this complex with 1.6 equiv of $pdmH_2$ in MeCN, followed by filtration and layering the resulting solution with Et_2O, affords crystalline $[Mn_9(O_2CEt)_{12}(pdm)(pdmH)_2(L)_2]$ (**2**) in 15% yield after several weeks. The use of more than 2 or less than 1.5 equiv of $pdmH_2$ reduces the yield of the final product. In addition, it was again not possible to isolate the $MeCO^-$ analogue of **2** in pure form from the analogous reaction with $[Mn_3O(O_2CMe)_6(py)_3][ClO_4]$, presumably due to its lower solubility.

The formation of **2** is summarized in eq 2 and also involves reduction of the Mn centers from an average oxidation state of +2.67 in the $Mn^{II}Mn^{III}_2$ starting complex to +2.22 in the $Mn^{II}_7Mn^{III}_2$ product, accompanied by fragmentation and structural rearrangement to yield the new complex. Again the hemiacetal ligand L^{2-} is formed in situ.

$$3\,[Mn_3O(O_2CEt)_6(py)_3] + 7\,pdmH_2 + 3\,EtCO_2H \rightarrow [Mn_9(O_2CEt)_{12}(pdm)(pdmH)_2(L)_2] + 9\,py + 3\,H_2O \quad (2)$$

A search of the chemical literature reveals that the compound most structurally similar to LH_2 whose synthesis as a discrete molecule has been reported is the related ether, 6-(6-hydroxymethylpyridin-2-ylmethoxymethyl)pyridin-2-yl]-methanol ($L'H_2$).[27] This preparation employs hmpH and 2-(chloromethyl)pyridine as the starting materials. A search of the Cambridge Crystallographic Database did not produce any X-ray structures of coordination compounds incorporating L′ as a ligand, and it seems likely that it has not been used for this purpose to date. It appears that both the formation of ligand L^{2-} and its coordination to a metal are unprecedented.

Structure Description of Complex 1. A labeled ORTEP plot of complex **1** is shown in Figure 1, together with stereoviews. Selected interatomic distances and angles are listed in Table 2. Complex **1** crystallizes in the monoclinic space group $P2_1/n$. The asymmetric unit consists of one-half of the octanuclear complex, one disordered $[ClO_4]^-$ anion, and disordered solvent. The cluster lies on an inversion center and thus manifests C_i point symmetry.

The structure of complex **1** contains a $[Mn^{II}_6Mn^{III}_2(\mu_4\text{-}O)_2(\mu_3\text{-}O)_4(\mu\text{-}O)_4]^{2+}$ core (Figure 3a), where the two μ_4-O atoms are O^{2-} ligands, the four μ_3-O atoms are from L^{2-} ligands, and the four μ-O atoms are from $EtCO_2^-$ ligands. The core can be considered as two distorted cubanes edge-

(25) Wernsdorfer, W. *Adv. Chem. Phys.* **2001**, *118*, 99.
(26) Boskovic, C.; Hendrickson, D. N.; Christou, G. Unpublished results.
(27) Newcomb, M.; Timko, J. M.; Wlaba, D, M.; Cram, D. J. *J. Am. Chem. Soc.* **1977**, *99*, 6392.

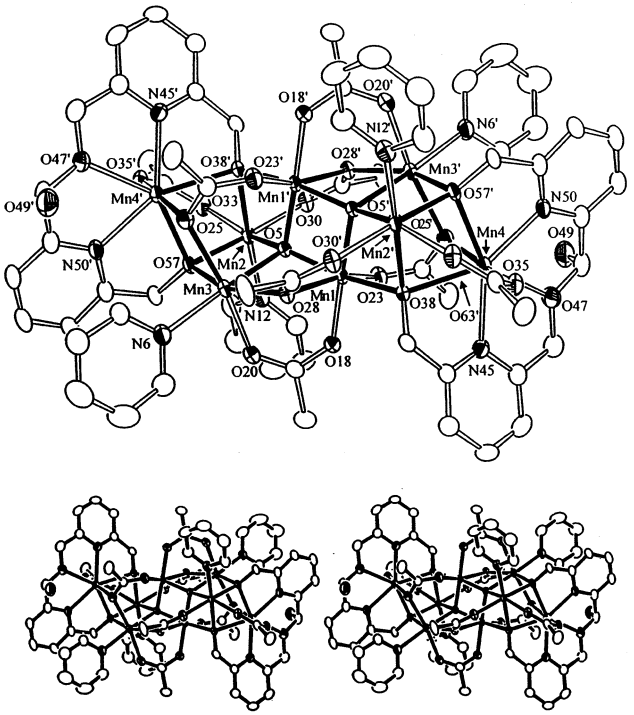

Figure 1. ORTEP representation of complex **1** at the 50% probability level, together with a stereopair; the methyl-C atoms of the $EtCO_2^-$ ligands are excluded for clarity.

linked together at the Mn(1)−O(5′) and Mn(1′)−O(5) edges, with O(28) and O(28′) providing additional bridges. Bond valence sum (BVS) calculations indicate that Mn(1) is Mn^{III}, while the remaining Mn centers are Mn^{II}. In addition Mn(1) displays Jahn−Teller (JT) elongation, typical of high-spin Mn^{III} (d^4), with the JT axis avoiding the O^{2-} ligands and lying on O(23) and O(28) from $EtCO_2^-$ ligands.

The peripheral ligation is provided by eight $EtCO_2^-$, four pyridine, and two L^{2-} ligands. Of the eight $EtCO_2^-$ ligands, four bind in the common μ mode and four bind in the less common μ_3 mode, with one O atom bridging two Mn centers and the other O atom terminal to a third Mn center. Each L^{2-} group ligates Mn(4) in a pentadentate manner through two N atoms and three O atoms, which occupy the five equatorial sites of a distorted pentagonal bipyramid. Within the equatorial plane, the Mn···O and Mn···N distances vary from 2.22 to 2.37 Å and the angles at Mn(4) vary from 66.8° to 81.6°. Although the pyridine rings of L^{2-} are individually planar, the pentadentate ligand itself is nonplanar, with intra-annular torsion angles of the four five-membered chelate rings varying from 3 to 38°. In addition, the two pyridine rings are distinctly tilted with respect to each other, at an angle of 33°. There is some crystallographic disorder in the free hydroxy group of each L^{2-} ligand, with O(49) disordered over the four sites, with the occupancy factors summing to 0.98. The axial sites of Mn(4) are occupied by O atoms from $EtCO_2^-$ ligands. In addition, one of the pyridine rings of each L^{2-} ligand [N(50)−C(55)] displays an intramolecular π-stacking interaction with one of the pyridine ligands [N(6′)−C(11′)] with a ring separation of ∼3.8 Å.

Complex **1** possesses a structure that is quite different from that of any previously structurally characterized octanuclear Mn-carboxylate complex. These complexes are $[Mn_8O_4(O_2CMe)_{12}(pic)_4]$ (picH = 2-picolinic acid),[28a] $[Mn_8O_4(O_2CPh)_{12}(Et_2mal)_2(H_2O)_2]^{2-}$ (Et_2malH_2 = 2,2-diethylmalonic acid),[28c,d] $[Mn_8O_6Cl_6(O_2CPh)_7(H_2O)_2]^-$,[29] $[Mn_4O_2(O_2CPh)_6(dbm)_2(bpe)]_2$ (dbmH = dibenzoylmethane, bpe = *trans*-1,2-bis(4-pyridyl)ethene),[30] and $[Mn_8O_4(O_2CEt)_{14}(L_2)_2]^{2+}$ (L_2 = a bis-2,2′-bipyridine ligand).[31]

Structure Description of Complex 2. A labeled ORTEP plot of complex **2**·0.2MeCN is shown in Figure 2, together with stereoviews. Selected interatomic distances and angles are listed in Table 3. Complex **1** crystallizes in the triclinic space group $P\bar{1}$. The asymmetric unit contains the entire enneanuclear complex in addition to solvent, and thus crystallographically complex **2** has C_1 point symmetry.

The complex contains a $[Mn^{II}_7Mn^{III}_2(\mu_3\text{-}O)_6(\mu\text{-}O)_6]^{4-}$ core (Figure 3b), where the six μ_3-O atoms are from L^{2-} and $pdmH^-$ ligands, while the six μ-O atoms are from pdm^{2-} and $EtCO_2^-$ ligands. Note that there are no O^{2-} ions in this cluster. The core can be considered as two distorted cubanes, each linked by two μ-O atoms to an additional Mn^{II} center, Mn(5). BVS calculations indicate that Mn(4) and Mn(6) are Mn^{III}, while the remaining Mn centers are Mn^{II}. In addition, Mn(4) and Mn(6) display JT elongation, with the JT axes lying on O(12) and O(17) for Mn(4) and O(20) and O(52) for Mn(6), where all of these O atoms are from $EtCO_2^-$ ligands.

The peripheral ligation is composed of 12 $EtCO_2^-$, two $pdmH^-$, one pdm^{2-}, and two L^{2-} ligands, with three different binding modes observed for the $EtCO_2^-$ ligands and also three distinct binding modes observed for the ligands derived from $pdmH_2$. Six of the $EtCO_2^-$ ligands bind in the usual μ mode, four bind in the less common μ_3 mode, and two bind in a monodentate fashion. The "dangling" O atoms of the monodentate $EtCO_2^-$ ligands participate in intramolecular hydrogen bonds with the "dangling" O atoms of the two $pdmH^-$ ligands. The hydrogen bond distances are 2.61 Å for both O(62)···O(89) and O(67)···O(99). These $pdmH^-$ ligands bind in a μ_3 fashion, with the other O atoms [O(80) and O(90)] bridging three Mn atoms and also combining with the N atom to chelate one of these Mn atoms [Mn(3) and Mn(7)]. In addition, there is a single pdm^{2-} ligand, which serves as the sole bridge between the two distorted cubane units. This ligand binds in a μ_3 manner, with O(70) bridging Mn(4) and Mn(5), O(79) bridging Mn(5) and Mn(6), and N(77) binding in a terminal fashion to Mn(5), thus forming two chelate rings to Mn(5). Hence Mn(5) is actually seven-

(28) (a) Libby, E.; Folting, K.; Huffman, J. C.; Christou, G. *J. Am. Chem. Soc.* **1990**, *112*, 5354. (b) Libby, E.; Folting, K.; Huffman, C. J.; Huffman, J. C.; Christou, G. *Inorg. Chem.* **1993**, *32*, 2549. (c) Wemple, M. W.; Tsai, J. P. Streib, W. E.; Hendrickson, D. N.; Christou, G *Chem. Commun.* **1994**, 1031. (d) Wemple, M. W.; Tsai, H.-L.; Wang, S.; Claude, J. P. Streib, W. E.; Huffman, J. C.; Hendrickson, D. N.; Christou, G. *Inorg. Chem.* **1996**, *35*, 643.

(29) (a) Wang, S.; Huffman, J. C.; Folting, K.; Streib, W. E.; Lobkovsky, E. B.; Christou, G. *Angew. Chem., Int. Ed. Engl.* **1991**, *30*, 1672. (b) Tsai, H.-L.; Wang, S.; Folting, K.; Streib, W. E.; Hendrickson, D. N.; Christou, G. *J. Am. Chem. Soc.* **1995**, *117*, 2503.

(30) Wang, S.; Tsai, H.-L.; Folting, K.; Martin, J. D.; Hendrickson, D. N.; Christou, G. *Chem. Commun.* **1994**, 671.

(31) Grillo, V. A.; Knapp, M. J.; Bollinger, J. C.; Hendrickson, D. N.; Christou, G. *Angew. Chem., Int. Ed. Engl.* **1996**, *35*, 1818.

Table 2. Bond Distances (Å) and Angles (deg) for Complex **1**

Mn(1)	Mn(1′)	2.802(2)	Mn(2)	O(33)	2.135(3)		
Mn(1)	Mn(2)	3.921(2)	Mn(2)	O(38′)	2.322(3)		
Mn(1)	Mn(2′)	3.127(2)	Mn(2)	O(57)	2.171(3)		
Mn(1)	Mn(3)	3.196(2)	Mn(2)	N(12)	2.237(4)		
Mn(1)	Mn(3′)	3.461(2)	Mn(3)	O(5)	2.208(3)		
Mn(1)	Mn(4)	3.868(2)	Mn(3)	O(20)	2.145(3)		
Mn(2)	Mn(3)	3.361(2)	Mn(3)	O(25)	2.235(3)		
Mn(2)	Mn(4′)	3.268(2)	Mn(3)	O(28)	2.199(3)		
Mn(3)	Mn(4′)	3.382(2)	Mn(3)	O(57)	2.155(3)		
Mn(1)	O(5)	1.885(3)	Mn(3)	N(6)	2.270(4)		
Mn(1)	O(5′)	1.891(3)	Mn(4)	O(25′)	2.240(3)		
Mn(1)	O(18)	1.963(3)	Mn(4)	O(35)	2.135(3)		
Mn(1)	O(23)	2.259(3)	Mn(4)	O(38)	2.365(3)		
Mn(1)	O(28)	2.294(3)	Mn(4)	O(47)	2.383(3)		
Mn(1)	O(38)	1.964(3)	Mn(4)	O(57′)	2.216(3)		
Mn(2)	O(5)	2.212(3)	Mn(4)	N(45)	2.253(3)		
Mn(2)	O(30)	2.129(3)	Mn(4)	N(50)	2.253(3)		
O(5)	Mn(1)	O(5′)	84.21(11)	O(30)	Mn(2)	N(12)	90.03(12)
O(5)	Mn(1)	O(18)	98.12(11)	O(33)	Mn(2)	O(38′)	90.81(10)
O(5′)	Mn(1)	O(18)	177.61(11)	O(33)	Mn(2)	O(57)	92.74(10)
O(5)	Mn(1)	O(23)	91.76(11)	O(33)	Mn(2)	N(12)	91.13(12)
O(5)	Mn(1)	O(23)	101.67(11)	O(38′)	Mn(2)	O(57)	83.56(10)
O(5)	Mn(1)	O(28)	81.56(10)	O(38′)	Mn(2)	N(12)	177.89(11)
O(5′)	Mn(1)	O(28)	94.04(11)	O(57)	Mn(2)	N(12)	97.18(12)
O(5)	Mn(1)	O(38)	169.33(11)	O(5)	Mn(3)	O(20)	88.49(10)
O(5′)	Mn(1)	O(38)	85.85(11)	O(5)	Mn(3)	O(25)	96.06(10)
O(18)	Mn(1)	O(23)	78.82(11)	O(5)	Mn(3)	O(28)	77.24(10)
O(18)	Mn(1)	O(28)	85.82(11)	O(5)	Mn(3)	O(57)	79.33(10)
O(18)	Mn(1)	O(38)	91.79(11)	O(5)	Mn(3)	N(6)	176.40(12)
O(23)	Mn(1)	O(28)	162.24(10)	O(20)	Mn(3)	O(25)	171.89(10)
O(23)	Mn(1)	O(38)	94.04(11)	O(20)	Mn(3)	O(28)	88.86(10)
O(28)	Mn(1)	O(38)	95.31(11)	O(20)	Mn(3)	O(57)	93.67(11)
O(5)	Mn(2)	O(30)	94.76(10)	O(20)	Mn(3)	N(6)	87.93(13)
O(5)	Mn(2)	O(33)	160.27(10)	O(25)	Mn(3)	O(28)	98.68(10)
O(5)	Mn(2)	O(38′)	70.64(9)	O(25)	Mn(3)	O(57)	80.63(10)
O(5)	Mn(2)	O(57)	78.90(10)	O(25)	Mn(3)	N(6)	87.54(12)
O(5)	Mn(2)	N(12)	107.53(12)	O(28)	Mn(3)	O(57)	156.36(10)
O(30)	Mn(2)	O(33)	91.51(11)	O(28)	Mn(3)	N(6)	102.39(12)
O(30)	Mn(2)	O(38′)	89.09(10)	O(57)	Mn(3)	N(6)	101.19(11)
O(30)	Mn(2)	O(57)	171.56(11)	O(25′)	Mn(4)	O(35)	170.06(10)
O(25′)	Mn(4)	O(38)	83.42(10)	Mn(1′)	O(5)	Mn(3)	115.25(12)
O(25′)	Mn(4)	O(47)	93.36(11)	Mn(1)	O(5)	Mn(3)	102.19(12)
O(25′)	Mn(4)	O(57′)	79.22(10)	Mn(2)	O(5)	Mn(3)	99.04(9)
O(25′)	Mn(4)	N(45)	102.31(11)	Mn(3)	O(25)	Mn(4′)	98.21(11)
O(25′)	Mn(4)	N(50)	89.06(12)	Mn(1)	O(28)	Mn(3)	90.64(10)
O(35)	Mn(4)	O(38)	91.52(10)	Mn(1)	O(38)	Mn(2′)	93.34(10)
O(35)	Mn(4)	O(47)	96.14(11)	Mn(1)	O(38)	Mn(4)	126.35(13)
O(35)	Mn(4)	O(57′)	91.60(11)	Mn(2′)	O(38)	Mn(4)	88.42(9)
O(35)	Mn(4)	N(45)	84.05(12)	Mn(2)	O(57)	Mn(3)	101.97(10)
O(35)	Mn(4)	N(50)	91.99(12)	Mn(2)	O(57)	Mn(4′)	96.30(11)
O(38)	Mn(4)	O(47)	137.37(10)	Mn(3)	O(57)	Mn(4′)	101.39(11)
O(38)	Mn(4)	O(57′)	81.60(9)				
O(38)	Mn(4)	N(45)	71.44(10)				
O(38)	Mn(4)	N(50)	154.86(11)				
O(47)	Mn(4)	O(57′)	139.68(10)				
O(47)	Mn(4)	N(45)	67.79(11)				
O(47)	Mn(4)	N(50)	66.83(12)				
O(57′)	Mn(4)	N(45)	152.52(11)				
O(57′)	Mn(4)	N(50)	73.42(11)				
N(45)	Mn(4)	N(50)	133.69(13)				
Mn(1)	O(5)	Mn(1′)	95.79(11)				
Mn(1′)	O(5)	Mn(2)	99.21(12)				
Mn(1)	O(5)	Mn(2)	145.63(14)				

coordinate, possessing a distorted pentagonal bipyramidal geometry, with the equatorial plane comprising N(77), O(70), and O(79) from the pdm^{2-} ligand and O(17) and O(20) from μ_3-$EtCO_2^-$ ligands, and the axial positions are O(42) and O(45) from μ-$EtCO_2^-$ ligands. Finally, complex **2** possesses two pentadentate L^{2-} ligands binding to Mn(1) and Mn(9) in a manner similar to that observed in complex **1**. Within the pentagonal units of complex **2**, the Mn···O and Mn···N distances vary from 2.16 to 2.48 Å, and the angles at Mn(1) and Mn(9) vary from 66.4° to 78.5°. Again the pyridine rings of L^{2-} are individually planar, while the ligand itself is nonplanar, with intra-annular torsion angles of the four five-membered chelate rings varying from 1° to 42°, and the two pyridine rings tilted at angles of 24° and 21° with respect to each other for Mn(1) and Mn(9), respectively. There is again some crystallographic disorder in the free hydroxy group of each ligand, with the O atom disordered over the four sites with occupancy factors summing to 1.03 and 1.09 for Mn-

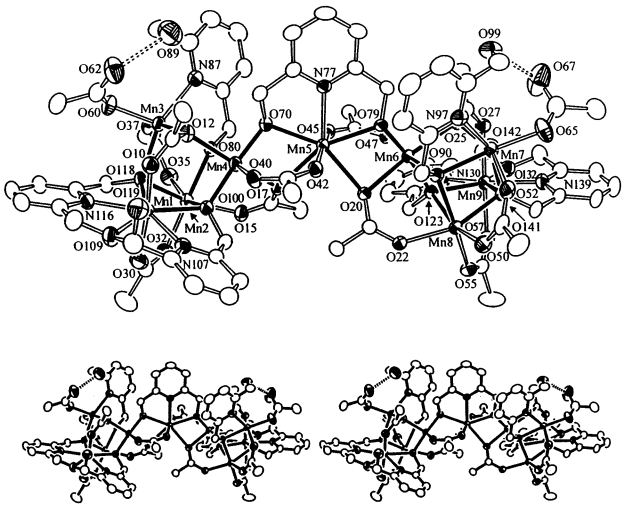

Figure 2. ORTEP representation of complex **2** at the 50% probability level, together with a stereopair; the methyl-C atoms of the $EtCO_2^-$ ligands are excluded for clarity.

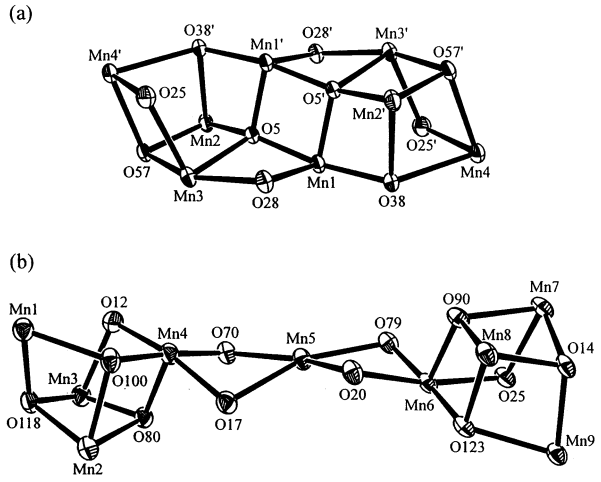

Figure 3. ORTEP representations of the cores of complexes **1** (a) and **2** (b) at the 50% probability level.

(1) and Mn(9), respectively. Again, the axial sites of Mn(1) and Mn(9) are occupied by O atoms from $EtCO_2^-$ ligands. Finally, although the molecule formally has no symmetry, there is approximate C_2 point symmetry, with the C_2 axis passing through Mn(5), N(77), and C(74). Note that with the −OH groups involved in *intra*molecular hydrogen bonding and with only a minor (and disordered) solvent content in the cell, complex **2** contains essentially isolated Mn_9 molecules.

Complex **2** also represents a structurally novel addition to the family of known enneanuclear Mn-carboxylate complexes. The other structurally characterized members of this family are $[Mn_9O_4(O_2CPh)_8(sal)(salH)_2(py)_2]$ ($salH_2$ = salicylic acid),[32] $[Mn_9M_2O_7(O_2CR)_{15}(X)_2]$ (M = Na, X = MeCN; M = K, X = RCO_2H),[29,33] and $[Mn_9O_7(O_2CPh)_{13}(py)_2]$.[34]

Magnetic Susceptibility Studies of Complex 1. Variable-temperature dc susceptibility measurements were performed on a microcrystalline powder sample of **1**·$5H_2O$, restrained in eicosane to prevent torquing, in a 10 kG field in the range 1.8−300 K (Figure 4). The $\chi_M T$ value of 24.5 cm^3 mol^{-1} K at 300 K decreases gradually with decreasing temperature to 4.3 cm^3 mol^{-1} K at 1.8 K. The spin-only ($g = 2$) value for a unit composed of noninteracting $Mn^{II}_6Mn^{III}_2$ ions is 32.2 cm^3 mol^{-1} K. Hence, the molecule appears to possess appreciable intramolecular antiferromagnetic interactions.

Complex **1** contains six Mn^{II} and two Mn^{III} centers, with total spin values ranging from 0 to 19. Owing to the size and low symmetry of the molecule, it is not possible to apply the Kambe method[35] or otherwise evaluate the exchange parameters between the Mn ions. Thus, to determine the ground state of the complex, magnetization data were collected in the magnetic field and temperature ranges 1−70 kG and 1.8−4.0 K for complex **1**·$5H_2O$. However, it was not possible to obtain a good fit for these data assuming that only the ground state is populated in this temperature range. This suggests that low-lying excited states are populated, even at these relatively low temperatures. Thus, in an additional effort to determine the spin ground state of complex **1**·$5H_2O$, ac susceptibility measurements were performed with a 3.5 G ac field oscillating at 997 Hz. The ac data are essentially superimposable with the dc data and appear to be heading for $\chi_M T < 3$ cm^3 mol^{-1} K at 0 K (Figure 5). This is consistent with a small ground state spin value, probably $S = 0$, with very low-lying excited states that are populated even at 1.8 K.

The apparent $S = 0$ spin ground state indicated for complex **1** is not surprising given its structural relationship to the family of compounds of formula $[Mn_6(O_2CPh)_{10}(L'')_4]$ (L″ = py, MeCN), which have also been found to have $S = 0$.[36] The $[Mn^{II}_4Mn^{III}_2O_2]^{10+}$ core of these complexes is conserved in **1** (involving Mn(1), Mn(2), Mn(3), O(5)). The most dominant exchange interaction within this unit is undoubtedly a strong antiferromagnetic coupling between the bis(μ-O)-bridged Mn^{III} centers, Mn(1) and Mn(1′); the analogous interaction in the hexanuclear complex was found[36a] to have $J = -42$ cm^{-1}. In addition to this $[Mn^{II}_4Mn^{III}_2O_2]^{10+}$ fragment, complex **1** possesses two additional Mn^{II} centers [Mn(4)] at either extreme of each of the distorted cubane units. Typically, $Mn^{II}-Mn^{II}$ and $Mn^{II}-Mn^{III}$ exchange interactions are weak and antiferromagnetic.[36b] Thus, whatever is the resultant spin of each half of **1**, the strong antiferromagnetic coupling at the central $[Mn^{III}_2O_2]$ unit will give a $S = 0$ ground state for the complete molecule. In addition, the population of low-lying excited states for complex **1**, even at low temperatures, is not unexpected, as the complex $[Mn_6(O_2CPh)_{10}(py)_2(MeCN)_2]$ has $S = 1$ excited states only 4 cm^{-1} above the $S = 0$ ground state,[36a] and even lower-lying excited states are probable for **1**, given its greater

(32) (a) Christmas, C.; Vincent, J. B.; Huffman, J. C.; Christou, G.; Chang, H.-R.; Hendrickson, D. N. *Angew. Chem., Int. Ed. Engl.* **1987**, *26*, 915. (b) Christmas, C.; Vincent, J. B.; Chang, H.-R.; Huffman, J. C.; Christou, G.; Hendrickson, D. N. *J. Am. Chem. Soc.* **1988**, *110*, 823.
(33) Murrie, M.; Parsons, S.; Winpenny, R. E. P. *J. Chem. Soc., Dalton Trans.* **1998**, 1423.
(34) Low, D. W.; Eichorn, D. M.; Draganescu, A.; Armstrong, W. H. *Inorg. Chem.* **1991**, *30*, 878.
(35) Kambe, K. J. *Phys. Soc. Jpn.* **1950**, *48*, 15.
(36) (a) Schake, A. R.; Vincent, J. B.; Li, Q.; Boyd, P. D. W.; Folting, K.; Huffman, J. C.; Hendrickson, D. N.; Christou, G. *Inorg. Chem.* **1989**, *28*, 1915. (b) Que, L.; True, A. E. *Prog. Inorg. Chem.* **1990**, *38*, 97.

Table 3. Bond Distances (Å) and Angles (deg) for Complex **2**

Mn(1)	Mn(2)	3.330(2)	Mn(1)	N(116)	2.232(3)		
Mn(1)	Mn(3)	3.699(2)	Mn(2)	O(15)	2.168(3)		
Mn(1)	Mn(4)	3.720(2)	Mn(2)	O(32)	2.094(3)		
Mn(2)	Mn(3)	3.278(2)	Mn(2)	O(35)	2.124(3)		
Mn(2)	Mn(4)	3.210(2)	Mn(2)	O(80)	2.249(2)		
Mn(3)	Mn(4)	3.366(2)	Mn(2)	O(100)	2.301(2)		
Mn(4)	Mn(5)	3.335(2)	Mn(2)	O(118)	2.211(2)		
Mn(5)	Mn(6)	3.316(2)	Mn(3)	O(12)	2.241(3)		
Mn(6)	Mn(7)	3.386(2)	Mn(3)	O(37)	2.178(3)		
Mn(6)	Mn(8)	3.192(2)	Mn(3)	O(60)	2.073(3)		
Mn(6)	Mn(9)	3.720(2)	Mn(3)	O(80)	2.213(2)		
Mn(7)	Mn(8)	3.263(2)	Mn(3)	O(118)	2.208(2)		
Mn(7)	Mn(9)	3.733(2)	Mn(3)	N(87)	2.300(3)		
Mn(8)	Mn(9)	3.330(2)	Mn(4)	O(12)	2.235(3)		
Mn(1)	O(10)	2.216(3)	Mn(4)	O(17)	2.196(2)		
Mn(1)	O(30)	2.190(3)	Mn(4)	O(40)	1.947(2)		
Mn(1)	O(100)	2.305(2)	Mn(4)	O(70)	1.863(2)		
Mn(1)	O(109)	2.473(3)	Mn(4)	O(80)	1.951(2)		
Mn(1)	O(118)	2.163(2)	Mn(4)	O(100)	1.939(2)		
Mn(1)	N(107)	2.237(3)	Mn(5)	O(17)	2.478(2)		
Mn(5)	O(20)	2.3853(2)	Mn(7)	N(97)	2.328(3)		
Mn(5)	O(42)	2.160(2)	Mn(8)	O(22)	2.168(2)		
Mn(5)	O(45)	2.149(2)	Mn(8)	O(50)	2.103(3)		
Mn(5)	O(70)	2.264(2)	Mn(8)	O(55)	2.091(3)		
Mn(5)	O(79)	2.285(2)	Mn(8)	O(90)	2.238(3)		
Mn(5)	N(77)	2.289(3)	Mn(8)	O(123)	2.293(2)		
Mn(6)	O(20)	2.215(2)	Mn(8)	O(141)	2.211(2)		
Mn(6)	O(25)	2.234(2)	Mn(9)	O(27)	2.186(2)		
Mn(6)	O(47)	1.951(2)	Mn(9)	O(57)	2.165(2)		
Mn(6)	O(79)	1.863(2)	Mn(9)	O(123)	2.317(2)		
Mn(6)	O(90)	1.948(2)	Mn(9)	O(132)	2.479(3)		
Mn(6)	O(123)	1.934(2)	Mn(9)	O(141)	2.184(2)		
Mn(7)	O(25)	2.275(2)	Mn(9)	N(130)	2.239(3)		
Mn(7)	O(52)	2.196(2)	Mn(9)	N(139)	2.220(3)		
Mn(7)	O(65)	2.073(3)					
Mn(7)	O(90)	2.216(2)					
Mn(7)	O(141)	2.182(2)					
O(10)	Mn(1)	O(30)	7.82(1)	O(15)	Mn(2)	O(35)	102.61(10)
O(10)	Mn(1)	O(100)	97.94(9)	O(15)	Mn(2)	O(100)	83.08(9)
O(10)	Mn(1)	O(109)	76.75(9)	O(15)	Mn(2)	O(118)	157.82(9)
O(10)	Mn(1)	O(118)	101.57(9)	O(32)	Mn(2)	O(35)	102.21(11)
O(10)	Mn(1)	N(107)	86.85(10)	O(32)	Mn(2)	O(80)	167.43(10)
O(10)	Mn(1)	N(116)	89.76(11)	O(32)	Mn(2)	O(100)	95.51(10)
O(30)	Mn(1)	O(100)	90.31(10)	O(32)	Mn(2)	O(118)	92.92(10)
O(30)	Mn(1)	N(107)	87.05(1)	O(35)	Mn(2)	O(80)	89.50(9)
O(30)	Mn(1)	O(109)	91.16(10)	O(35)	Mn(2)	O(100)	160.06(10)
O(30)	Mn(1)	N(116)	86.69(1)	O(35)	Mn(2)	O(118)	92.26(10)
O(30)	Mn(1)	O(118)	88.81(10)	O(80)	Mn(2)	O(100)	72.23(8)
O(100)	Mn(1)	O(109)	139.87(9)	O(80)	Mn(2)	O(118)	81.94(8)
O(100)	Mn(1)	O(118)	78.48(8)	O(100)	Mn(2)	O(118)	77.63(8)
O(100)	Mn(1)	N(107)	72.79(10)	O(12)	Mn(3)	O(37)	159.41(9)
O(100)	Mn(1)	N(116)	153.73(10)	O(12)	Mn(3)	O(60)	98.53(10)
O(109)	Mn(1)	O(118)	141.65(9)	O(12)	Mn(3)	O(80)	74.34(9)
O(109)	Mn(1)	N(107)	67.24(10)	O(12)	Mn(3)	O(118)	89.62(9)
O(109)	Mn(1)	N(116)	66.35(10)	O(12)	Mn(3)	N(87)	94.96(10)
O(118)	Mn(1)	N(107)	150.94(10)	O(37)	Mn(3)	O(60)	101.51(10)
O(118)	Mn(1)	N(116)	75.37(10)	O(37)	Mn(3)	O(80)	85.24(9)
N(107)	Mn(1)	N(116)	132.97(11)	O(37)	Mn(3)	O(118)	85.13(9)
O(15)	Mn(2)	O(32)	99.77(10)	O(37)	Mn(3)	N(87)	81.66(11)
O(15)	Mn(2)	O(80)	81.84(9)	O(60)	Mn(3)	O(80)	170.99(10)
O(60)	Mn(3)	O(118)	91.75(10)	O(17)	Mn(5)	O(70)	68.26(8)
O(60)	Mn(3)	N(87)	112.67(12)	O(17)	Mn(5)	O(79)	152.14(8)
O(80)	Mn(3)	O(118)	82.82(9)	O(17)	Mn(5)	N(77)	137.16(9)
O(80)	Mn(3)	N(87)	73.97(10)	O(20)	Mn(5)	O(42)	85.82(9)
O(118)	Mn(3)	N(87)	154.08(11)	O(20)	Mn(5)	O(45)	87.88(9)
O(12)	Mn(4)	O(17)	168.09(9)	O(20)	Mn(5)	O(70)	151.07(8)
O(12)	Mn(4)	O(40)	92.82(10)	O(20)	Mn(5)	O(79)	69.83(8)
O(12)	Mn(4)	O(70)	95.46(10)	O(20)	Mn(5)	N(77)	138.25(9)
O(12)	Mn(4)	O(80)	79.72(9)	O(42)	Mn(5)	O(45)	170.74(9)
O(12)	Mn(4)	O(100)	89.68(9)	O(42)	Mn(5)	O(70)	83.71(9)
O(17)	Mn(4)	O(40)	98.83(10)	O(42)	Mn(5)	O(79)	100.17(9)
O(17)	Mn(4)	O(70)	81.67(10)	O(42)	Mn(5)	N(77)	94.58(10)
O(17)	Mn(4)	O(80)	88.78(9)	O(45)	Mn(5)	O(70)	98.72(9)
O(17)	Mn(4)	O(100)	92.86(10)	O(45)	Mn(5)	O(79)	83.96(8)
O(40)	Mn(4)	O(70)	92.34(10)	O(45)	Mn(5)	N(77)	94.63(9)
O(40)	Mn(4)	O(80)	171.88(10)	O(70)	Mn(5)	O(79)	138.66(8)
O(40)	Mn(4)	O(100)	89.59(10)	O(70)	Mn(5)	N(77)	69.63(9)
O(70)	Mn(4)	O(80)	91.57(10)	O(79)	Mn(5)	N(77)	69.03(9)
O(70)	Mn(4)	O(100)	174.42(11)	O(20)	Mn(6)	O(25)	168.02(8)
O(80)	Mn(4)	O(100)	87.17(9)	O(20)	Mn(6)	O(47)	98.48(9)
O(17)	Mn(5)	O(20)	84.58(8)	O(20)	Mn(6)	O(79)	81.47(9)
O(17)	Mn(5)	O(42)	88.39(9)	O(20)	Mn(6)	O(90)	88.40(9)
O(17)	Mn(5)	O(45)	84.27(8)	O(20)	Mn(6)	O(123)	91.54(9)
O(25)	Mn(6)	O(47)	93.43(9)	O(90)	Mn(7)	N(97)	74.04(10)
O(25)	Mn(6)	O(79)	96.92(9)	O(141)	Mn(7)	N(97)	156.43(10)
O(25)	Mn(6)	O(90)	79.78(9)	O(22)	Mn(8)	O(50)	103.70(10)
O(25)	Mn(6)	O(123)	89.89(9)	O(22)	Mn(8)	O(55)	96.14(10)
O(47)	Mn(6)	O(79)	91.72(10)	O(22)	Mn(8)	O(90)	82.94(9)
O(47)	Mn(6)	O(90)	172.56(10)	O(22)	Mn(8)	O(123)	83.68(8)
O(47)	Mn(6)	O(123)	89.43(9)	O(22)	Mn(8)	O(141)	159.04(9)

Table 3. Continued.

O(79)	Mn(6)	O(90)	92.10(10)	O(50)	Mn(8)	O(55)	101.59(10)
O(79)	Mn(6)	O(123)	173.02(10)	O(50)	Mn(8)	O(90)	90.60(9)
O(90)	Mn(6)	O(123)	87.55(9)	O(50)	Mn(8)	O(123)	160.97(10)
O(25)	Mn(7)	O(52)	158.69(9)	O(50)	Mn(8)	O(141)	90.63(9)
O(25)	Mn(7)	O(65)	108.55(11)	O(55)	Mn(8)	O(90)	167.62(9)
O(25)	Mn(7)	O(90)	73.60(8)	O(55)	Mn(8)	O(123)	94.92(9)
O(25)	Mn(7)	O(141)	88.30(8)	O(55)	Mn(8)	O(141)	95.84(9)
O(25)	Mn(7)	N(97)	89.49(9)	O(90)	Mn(8)	O(123)	72.70(8)
O(52)	Mn(7)	O(65)	92.55(11)	O(90)	Mn(8)	O(141)	81.68(9)
O(52)	Mn(7)	O(90)	85.14(9)	O(123)	Mn(8)	O(141)	78.21(8)
O(52)	Mn(7)	O(141)	87.54(9)	O(27)	Mn(9)	O(57)	168.99(10)
O(52)	Mn(7)	N(97)	86.05(10)	O(27)	Mn(9)	O(123)	98.10(9)
O(65)	Mn(7)	O(90)	175.50(11)	O(27)	Mn(9)	O(132)	77.19(9)
O(65)	Mn(7)	O(141)	93.22(10)	O(27)	Mn(9)	O(141)	100.63(9)
O(65)	Mn(7)	N(97)	109.70(12)	O(27)	Mn(9)	N(130)	85.53(10)
O(90)	Mn(7)	O(141)	82.83(9)	O(27)	Mn(9)	N(139)	89.72(10)
O(57)	Mn(9)	O(123)	87.68(9)	Mn(3)	O(80)	Mn(4)	107.71(11)
O(57)	Mn(9)	O(132)	92.32(9)	Mn(6)	O(90)	Mn(7)	108.62(10)
O(57)	Mn(9)	O(141)	89.68(9)	Mn(6)	O(90)	Mn(8)	99.14(10)
O(57)	Mn(9)	N(130)	87.28(10)	Mn(7)	O(90)	Mn(8)	94.18(9)
O(57)	Mn(9)	N(139)	89.23(10)	Mn(1)	O(100)	Mn(2)	92.59(8)
O(123)	Mn(9)	O(132)	139.55(8)	Mn(1)	O(100)	Mn(4)	122.19(12)
O(123)	Mn(9)	O(141)	78.24(8)	Mn(2)	O(100)	Mn(4)	98.03(9)
O(123)	Mn(9)	N(130)	72.74(10)	Mn(1)	O(118)	Mn(2)	99.18(9)
O(123)	Mn(9)	N(139)	153.22(10)	Mn(1)	O(118)	Mn(3)	115.63(11)
O(132)	Mn(9)	O(141)	142.20(9)	Mn(2)	O(118)	Mn(3)	95.78(9)
O(132)	Mn(9)	N(130)	66.87(10)	Mn(6)	O(123)	Mn(8)	97.71(9)
O(132)	Mn(9)	N(139)	67.15(10)	Mn(6)	O(123)	Mn(9)	121.87(11)
O(141)	Mn(9)	N(130)	150.91(10)	Mn(8)	O(123)	Mn(9)	92.48(8)
O(141)	Mn(9)	N(139)	75.14(10)	Mn(7)	O(141)	Mn(8)	95.91(9)
N(130)	Mn(9)	N(139)	133.67(12)	Mn(7)	O(141)	Mn(9)	117.51(10)
Mn(3)	O(12)	Mn(4)	97.54(9)	Mn(8)	O(141)	Mn(9)	98.50(9)
Mn(4)	O(17)	Mn(5)	90.85(9)				
Mn(5)	O(20)	Mn(6)	92.15(8)				
Mn(6)	O(25)	Mn(7)	97.34(9)				
Mn(4)	O(70)	Mn(5)	107.44(11)				
Mn(5)	O(79)	Mn(6)	105.69(10)				
Mn(2)	O(80)	Mn(3)	94.55(8)				
Mn(2)	O(80)	Mn(4)	99.44(9)				

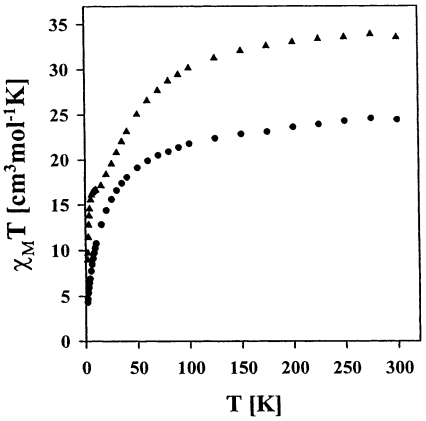

Figure 4. Plot of $\chi_M T$ vs temperature for microcrystalline samples of complex **1**·5H$_2$O (●) and **2** (▲) in eicosane. χ_M is the dc magnetic susceptibilty measured in a 10 kG field.

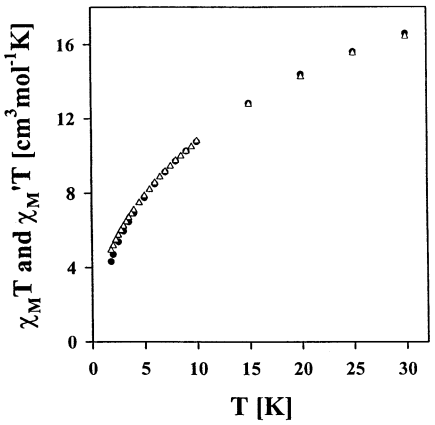

Figure 5. Plot of $\chi'_M T$ vs temperature for complex **1**·5H$_2$O in the 2.0−30 K range from ac magnetic susceptibility measurements (△) and including the dc $\chi_M T$ data (●) from Figure 4 for this temperature range. The ac data were measured with a 3.5 G ac field oscillating at 997 Hz, and χ_M is the dc magnetic susceptibilty measured in a 10 kG field.

nuclearity and extra Mn^{II} content. This situation is not uncommon in large Mn$_x$ clusters with $S = 0$, with both [Mn$_{10}$O$_8$(O$_2$CPh)$_6$(pic)$_8$] and [Mn$_{18}$O$_{16}$(O$_2$CPh)$_{22}$(phth)$_2$(H$_2$O)$_4$]$^{4-}$ (phthH = phthalic acid), for example, possessing $S = 0$ ground states and displaying evidence for low-lying excited states.[37,38]

Magnetic Susceptibility Studies of Complex 2. Variable-temperature dc susceptibility measurements were performed on a microcrystalline powder sample of **2**, restrained in eicosane to prevent torquing, in a 10 kG field in the range 1.8−300 K (Figure 4). The $\chi_M T$ value of 34.5 cm^3 mol^{-1} K at 300 K decreases gradually as the temperature is decreased to 15 K, before leveling out at ∼17 cm^3 mol^{-1} K and then rapidly decreasing below 5 K to a value of 8.9 cm^3 mol^{-1} K at 1.8 K. The spin-only ($g = 2$) value for a unit composed of noninteracting Mn$^{II}_7$Mn$^{III}_2$ ions is 36.6 cm^3 mol^{-1} K. Hence, the molecule appears to possess intramolecular antiferromagnetic interactions causing the decrease in $\chi_M T$, with the rapid decrease at temperatures below 5 K assigned to some combination of zero-field-splitting (ZFS), Zeeman effects, and intermolecular interactions.

(37) Eppley, H. J.; Aubin, S. M. J.; Streib, W. E.; Bollinger, J. C.; Hendrickson, D. N.; Christou, G. *Inorg. Chem.* **1997**, *36*, 109.
(38) Squire, R. C.; Aubin, S. M. J.; Folting, K.; Streib, W. E.; Christou, G.; Hendrickson, D. N. *Inorg. Chem.* **1995**, *34*, 6463.

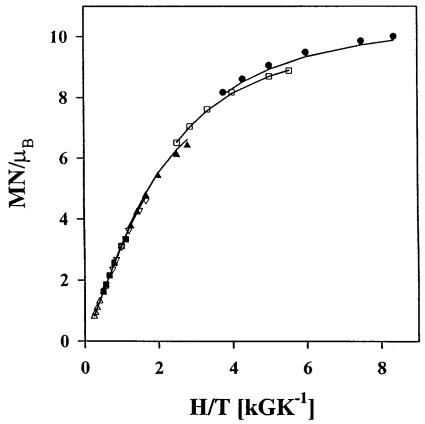

Figure 6. Plot of $M/N\mu_B$ vs H/T for complex **2** in eicosane at 1 (△), 2 (■), 3 (▽), 5 (▲), 10 (□), and 15 (●) kG. The solid lines are fits using the appropriate method; see the text for fitting parameters.

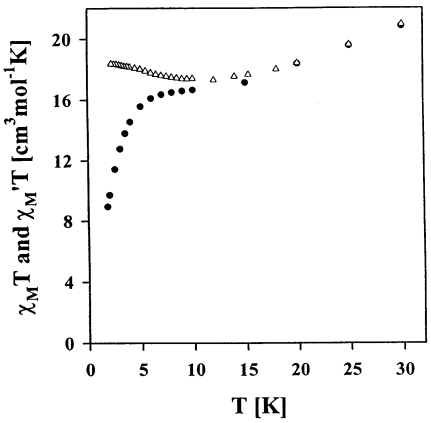

Figure 7. Plot of χ'_MT vs temperature for complex **2** in the 2.0−30 K range from ac magnetic susceptibility measurements (△) and including the dc χ_MT data (●) from Figure 4 for this temperature range. The ac data were measured with a 3.5 G ac field oscillating at 997 Hz, and χ_M is the dc magnetic susceptibilty measured in a 10 kG field.

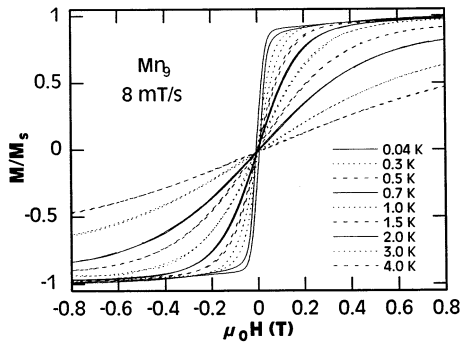

Figure 8. Plot of magnetization (normalized to the saturation magnetization M_s) vs applied field for complex **2** in the 0.04−4.0 K range at a sweep rate of 8 mT/s.

Complex **2** contains seven Mn^{II} and two Mn^{III} centers with the total spin values ranging from 1/2 to 43/2. Again, it is not possible to evaluate the various exchange parameters. To determine the ground state, magnetization data were collected in the 1−70 kG and 1.8−4.0 K range for complex **2**. The data in the range 1−15 kG are plotted as reduced magnetization ($M/N\mu_B$) versus H/T in Figure 6, where N is Avogadro's number and μ_B is the Bohr magneton. For a system occupying only the ground state and experiencing no ZFS, the various isofield lines would be superimposed and $M/N\mu_B$ would saturate at a value of gS. The nonsuperposition of the isofield lines clearly indicates ZFS. The data in the field range 1−15 kG were least-squares-fit using the methods described elsewhere,[22] involving a full diagonalization of the spin Hamiltonian matrix including axial ZFS and Zeeman interactions and assuming that only the ground state is populated. This produced a best fit with $S = 11/2$, $g = 2.0$, and $D = -0.11$ cm^{-1}, where D is the axial ZFS parameter. Attempts to fit the data using $S = 13/2$ or 9/2 resulted in unreasonable values for g ($g < 1.8$ and $g > 2.2$). When the data collected at fields >15 kG were included, the fits were not as good. This suggests that low-energy excited states with $S > 11/2$ are populated, even at these relatively low temperatures. As for the $S = 0$ situation mentioned above, this is also a common problem in higher nuclearity Mn_x systems with $S > 0$, for example, $[Mn_{30}O_{24}(OH)_8(O_2CCH_2{}^tBu)_{32}(H_2O)_2(CH_3NO_2)_4]$[39] and $[Mn_{12}O_8Cl_4(O_2CPh)_8(hmp)_6]$,[12] particularly when Mn^{II} ions are present as in these two examples, since these typically give weak exchange interactions and resulting small energy separations.

The $S = 11/2$ and $D = -0.11$ cm^{-1} values suggest that **2** should have an anisotropy barrier to magnetization reversal of $(S^2 - {}^1/_4)|D|$, or 3.3 cm^{-1} (4.7 K), which could be large enough to result in **2** displaying the slow magnetization relaxation characteristic of a single-molecule magnet (SMM). Thus, to both confirm the spin ground state of complex **1** and investigate the possibility of SMM behavior, ac susceptibility measurements were performed with a 3.5 G ac field oscillating at 997 Hz (Figure 7). The ac data are essentially superimposable with the dc data at temperatures above 15 K. However, as the temperature is further decreased, the value of $\chi_M'T$ increases slightly to give a value of 18.4 cm^3 mol^{-1} K at 1.8 K. This is consistent with an $S = 11/2$ spin ground state (17.9 cm^3 mol^{-1} K for $g = 2$). No signal was observed in the out-of-phase susceptibility (χ_M'') at temperatures down to 1.8 K, suggesting that the barrier to magnetization relaxation is too small to give a nonzero χ_M'' signal characteristic of a SMM. However, it was possible that **2** might still exhibit SMM behavior at even lower temperatures, and dc magnetization measurements were therefore performed at <1.8 K using a micro-SQUID apparatus.

Direct Current Magnetization Studies below 1.8 K. If complex **2** is a SMM below some temperature, then it will exhibit a hysteresis loop in a magnetization versus dc field plot. Shown in Figure 8 are such magnetization versus field scans for **2** at different temperatures in the 0.04−4.0 K range and a constant sweep rate of 8 mT/s. Hysteresis is indeed observed, but only the 0.3 and 0.04 K scans show an overall hysteresis profile that can be assigned as due to the anisotropy barrier to magnetization reversal. The butterfly-like pattern of the scans at higher temperature and the very slight hysteresis barely visible on some scans such as that at 1.0 K are characteristic, not of single-molecule magnetism behavior, but of a phonon-bottleneck; that is, phonon exchange

(39) Soler M.; Rumberger, E.; Folting, K.; Hendrickson, D. N.; Christou, G. *Polyhedron* **2001**, *20*, 1365.

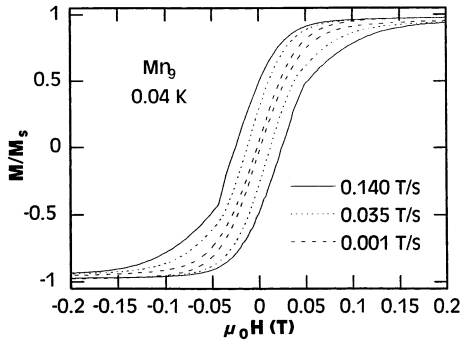

Figure 9. Normalized magnetization vs field hysteresis loops for complex **2** at 0.04 K at the three sweep rates shown.

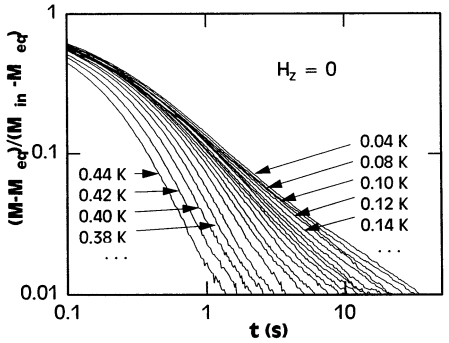

Figure 10. Magnetization vs time plots for complex **2** in zero applied field in the temperature range 0.04−0.44 K. The data for the upper and lower temperatures are indicated.

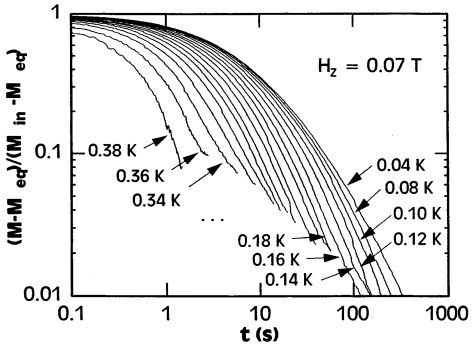

Figure 11. Magnetization vs time plots for complex **2** in an applied field of 0.07 T in the temperature range 0.04−0.38 K. The data for the upper and lower temperatures are indicated.

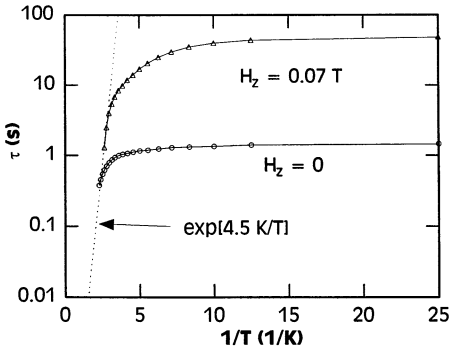

Figure 12. Arrhenius plots of relaxation time (τ) vs $1/T$ for complex **2** using the relaxation data in Figures 11 and 12. The dashed line corresponds to $\exp(U_{eff}/T)$, where U_{eff} is the effective barrier to magnetization relaxation.

(thermal coupling) between the crystal and its environment (cryostat) is limited, an equilibrium in the phonon density of states cannot be maintained during spin relaxation, and thus the latter is hampered and a small hysteresis is observed. This behavior was first described in a molecular system for a V_{15} cluster with $S = 1/2$.[40]

However, at the lowest temperature scans of Figure 8, true hysteresis due to an anisotropy barrier to magnetization relaxation is observed. This is more clearly seen in Figure 9, where the sweep rate is varied at a constant temperature of 0.04 K. The coercivity increases with sweep rate, as expected for a molecular species exhibiting slow magnetization relaxation, i.e., a SMM. The hysteresis loops do not show clear evidence of steps that would indicate the presence of resonant quantum tunneling of magnetization through the anisotropy barrier, as seen for other SMMs. The loops are not completely smooth, however, and it is likely that steps are present but are smeared out by a combination of broadening effects from intermolecular interactions and/or the distribution of molecular environments arising from the disordered ligands, as well as crystal defects.

To determine the effective barrier (U_{eff}) to magnetization reversal, magnetization relaxation measurements were performed.[6c,9b,41] The sample was first saturated in a field of −1 T, the field ramped at 0.28 T/s to the value at which the relaxation rate was to be measured, and the magnetization then followed as a function of time. The results are shown in Figures 10 and 11 for constant applied fields of zero and 0.07 T, respectively. The magnetization is plotted as $(M - M_{eq})/(M_{in} - M_{eq})$, where M_{in} is the initial magnetization, M_{eq} is the final, equilibrium magnetization, and M is the magnetization at time t. The relaxation time (τ) was determined for each temperature from data collected during the time required for a 90% decrease in the difference between M_{in} and M_{eq}, that is, until $(M - M_{eq})/(M_{in} - M_{eq}) = 0.1$. A plot of τ versus $1/T$ is shown for **2** in Figure 12. Two points immediately become obvious: (i) the relaxation time becomes temperature-independent at very low temperature, and (ii) the relaxation is faster at zero field than in a field of 0.07 T. These observations are consistent with the presence of resonant quantum tunneling of magnetization at zero field,[5,41] where the energies of M_s levels on one side of the anisotropy barrier are degenerate with those on the other. From the slope of the thermally activated region of the plot (dashed line in Figure 12) can be determined that $U_{eff} = 4.5$ K. This is the effective barrier to magnetization reversal and may be compared with the value calculated for the barrier (U) from the $S = 11/2$ and $D = -0.11$ cm^{-1} $= -0.16$ K values obtained from the dc magnetization fit of Figure 6; the calculated U is $(S^2 - {}^1/_4)|D| = 4.7$ K. Thus, $U_{eff} < U$, as expected in the presence of quantum tunneling via one of the higher energy M_s levels.[5] The temperature-independent relaxation rate below approximately 0.2 K is 0.7 s^{-1}.

(40) Chiorescu, I.; Wernsdorfer, W.; Muller, A.; Bogge, H.; Barbara, B. *Phys. Rev. Lett.* **2000**, *84*, 3454.
(41) Sangregorio, C.; Ohm, T.; Paulsen, C.; Sessoli, R.; Gatteschi, D. *Phys. Rev. Lett.* **1997**, *78*, 4045.

Discussion

The reactions of the Mn^{III}_3 and $Mn^{II}Mn^{III}_2$ trinuclear complexes $[Mn_3O(O_2CEt)_6(py)_3]^+$ and $[Mn_3O(O_2CEt)_6(py)_3]$ with $pdmH_2$ have afforded two new Mn-carboxylate clusters $[Mn_8O_2(py)_4(O_2CEt)_8(L)_2]^{2+}$ (**1**) and $[Mn_9(O_2CEt)_{12}(pdm)(pdmH)_2(L)_2]$ (**2**), which have been crystallographically characterized. Both of these complexes are new structural types, and both represent new ways in which distorted cubane units can be linked together. In addition, they both feature a novel pentadentate ligand that is formed in situ during the reaction. In the course of the reaction, some of the Mn^{III} centers are reduced to Mn^{II}, accompanied by oxidation of some of the $pdmH_2$ to the aldehyde. The product of the latter process is protonated in the acidic environment and undergoes nucleophilic attack from the alcohol moiety of some of the remaining $pdmH_2$ to form the hemiacetal, which then acts as a pentadentate ligand. In addition, complex **2** is unusual in that it possesses three different binding modes for the ligands derived by deprotonation of $pdmH_2$ within the one molecule.

Complexes **1** and **2** are both mixed-valent Mn^{II}/Mn^{III} and possess spin ground states of 0 and 11/2, respectively. A ground state with $S = 0$ is not unexpected for **1**, given its structural correspondence with the $[Mn_6(O_2CPh)_{10}(L'')_4]$ family of complexes with $S = 0$.[36a] The large number of competing $Mn^{II}-Mn^{II}$ and $Mn^{II}-Mn^{III}$ pairwise exchange interactions of similar magnitude lead to the $S = 11/2$ ground state for complex **2**. In addition, both complexes **1** and **2** possess low-lying excited states as expected from their high Mn^{2+} content, and these are populated even at very low temperatures.

A spin ground state of 11/2 is reasonably high, and complex **2** was therefore initially an attractive candidate for a new SMM. However, its low anisotropy as reflected in the D value of only -0.11 cm^{-1} (-0.16 K) means that the barrier to magnetization reversal is less than 5 K (given approximately by $(S^2 - {}^1/_4)|D|$ for a half-integer system in the absence of tunneling). The reason for the relatively small value of D is obvious from the structure of **2**. The main source of the molecular anisotropy will be the Jahn−Teller axially distorted Mn^{III} ions, of which there are only two; Mn^{II} is a fairly isotropic ion. The molecular anisotropy will thus be largely determined by the tensor summation of the Mn^{III} single-ion anisotropies, but the Mn^{III} Jahn−Teller axes, which will determine the single-ion anisotropy axes, are almost perpendicular in **2**, and the net consequence, therefore, is that the molecular anisotropy is low. Thus, the barrier to magnetization reversal is low, no out-of-phase (χ_M'') signal is observed above 1.8 K, and hysteresis loops are seen only at <0.4 K. Nevertheless, complex **2** is a new addition to the family of known single-molecule magnets.

The results for **2** may be compared with those of the family of Mn_4 SMMs with the $[Mn^{IV}Mn^{III}_3(\mu_3\text{-}O)_3(\mu_3\text{-}X)]^{6+}$ distorted-cubane core and a $S = 9/2$ ground state. Although their spin is slightly smaller than that of **2**, the anisotropy is greater ($D = -0.4$ to -0.6 cm^{-1}), and this leads to barriers approximately 2−3 times greater than for **2**, which in turn results in χ_M'' signals at ∼2 K and hysteresis loops up to ∼1 K.

Conclusions

The use of potentially bridging chelate ligands continues to represent a useful entry route into higher nuclearity Mn clusters. In the present work, the added chelate also functions as a reducing agent, and trapping of the oxidized form of the chelate within the Mn_x product has allowed a new pentadentate ligand to be identified.

Complex **2** has $S = 11/2$ and is a new member of the slowly growing family of SMMs. Unfortunately, the high content of isotropic Mn^{II} ions and the near-perpendicular arrangement of Mn^{III} Jahn−Teller axes results in a low barrier to magnetization reversal. Nevertheless, **2** provides a new SMM datum point for the continuing improvement of our understanding of this unusual magnetic phenomenon of single-molecule magnetism.

Acknowledgment. This work was supported by National Science Foundation grants to D.N.H. and G.C. A. Benoit, D. Mailly, and C. Thirion are acknowledged for help in the development of the micro-SQUID technique, and B. Barbara for his support.

Supporting Information Available: X-ray crystallographic files in CIF format for complexes **1** and **2**. This material is available free of charge via the Internet at http://pubs.acs.org.

IC020217P